Research Article

Mei Ai Tan, Cheow Keat Yeoh*, Pei Leng Teh, Nor Azura Abdul Rahim, Cheah Chie Song, and Chun Hong Voon

Effect of zinc oxide suspension on the overall filler content of the PLA/ZnO composites and cPLA/ZnO composites

https://doi.org/10.1515/epoly-2022-8113
received December 30, 2022; accepted April 10, 2023

Abstract: This work aimed to study the effect of zinc oxide (ZnO) filler suspension on the mechanical, electrical, and thermal properties of polylactic acid (PLA)/ZnO and cPLA/ZnO. Fused deposition modelling, one of the additive manufacturing methods, was used to fabricate the PLA specimen. PLA was used as the main material in this project, and the ZnO suspension was added during the printing process. The speed of the dispenser (low speed = 1,000 rpm, medium speed = 1,400 rpm, and high speed = 1,800 rpm) was the parameter that was varied to control the filler content of the composite. All the samples underwent a tensile test to determine the mechanical properties, followed by the scanning electron microscopy (SEM) test to analyse the fracture surface properties of the tensile test. SEM observations showed the PLA samples' inherent smooth appearance, but the PLA/ZnO composite showed a rougher surface. PLA and cPLA composites showed an enhanced storage modulus but lower loss modulus than the pure samples. Because of the high thermal and electrical conductivity of carbon black and ZnO, cPLA composites had higher electrical and thermal conductivity than PLA composites.

Keywords: 3D printing, additive manufacturing, composites, mechanical, electrical and thermal

*** Corresponding author: Cheow Keat Yeoh,** Faculty of Chemical Engineering Technology, University Malaysia Perlis, Malaysia; Centre of Excellence for Frontier Materials Research, University Malaysia Perlis, Arau, Perlis, Malaysia,
e-mail: ckyeoh@unimap.edu.my
Mei Ai Tan, Nor Azura Abdul Rahim, Cheah Chie Song: Faculty of Chemical Engineering Technology, University Malaysia Perlis, Arau, Perlis, Malaysia
Pei Leng Teh: Faculty of Chemical Engineering Technology, University Malaysia Perlis, Malaysia; Centre of Excellence for Frontier Materials Research, University Malaysia Perlis, Malaysia
Chun Hong Voon: Institute of Nano Electronic Engineering, University Malaysia Perlis, Arau, Perlis, Malaysia

1 Introduction

Polylactic acid (PLA) is a polyester polymerized from lactic acid (LA) with excellent biocompatibility and biodegradability (1). PLA resembles polypropylene, polyethylene, and polystyrene in terms of properties (2). It can be produced using currently available production equipment (2). PLA is generated from LA, often present in plants and animals as a metabolic byproduct or intermediate product. LA and hydrolytic breakdown products of PLA are harmless by nature (1). PLA is biologically degradable by common microorganisms after hydrolysis. Furthermore, the ease with which PLA melts upon heating enables some unique applications in 3D printing.

However, the poor mechanical properties of PLA can be improved by incorporating carbon fibre into the raw material. Carbon fibre will aid in strengthening the PLA because of its excellent mechanical characteristics, corrosion resistance, and high specific strength and modulus (3). Carbon fibre-reinforced PLA composites have higher flexural strength, flexural modulus, and flexural toughness than pure PLA composites by 11.82%, 16.82%, and 21.86%, respectively, based on previous research (4). To guarantee that the complete characteristics of 3D-printed CF-reinforced composites are enhanced, the interfacial properties of 3D-printed thermoplastic composites must be improved (5). PLA carbon fibre is a combination of 85% PLA and 15% carbon fibre to produce tougher PLA parts. They reported that additive manufacturing technology with CF polymer composites improved the strength and stiffness of many components. According to particular research, when CF is treated with concentrated nitric acid, the surface roughness of the CF rises, which improves the mechanical interlock and interfacial adhesion between CF and matrix (4).

In addition, the major disadvantage of these pure polymer materials is that they have poor mechanical characteristics, which include low tensile strength and

Young's modulus (6). As a result, reinforcing fillers are necessary so that the composite material may combine the benefits of the polymer matrix and fillers into a single material that can be used in various applications. Adding particle reinforcement to the polymer material is one of the effective ways to increase the mechanical characteristics of each material. There are many types of reinforcement, such as metal particles, carbon/graphene fibres, metal oxides, organic fillers, and other forms. Metal oxides have been found to have excellent physical and mechanical properties, as well as being inexpensive and simple to synthesize (7,8).

Inorganic fillers act as rigid fillers and nucleating agents, especially during annealing, to increase the crystallization of PLA and thus cause the modulus, tensile strength, and crystallinity to be higher (9). Controlling the ratio of two kinds of PLA is also an effective way to monitor the degradation of PLA (9). In addition, incorporating nanofillers, such as organo-modified layered silicates, silver, zinc oxide (ZnO), graphite derivatives, carbon nanotubes (CNTs), and silica, is a realistic and feasible approach for improving the antibacterial, barrier, thermal, and mechanical properties of PLA (9). However, the cost of silver restricts the application. Metal oxides like ZnO and TiO_2 are widely used in health-oriented applications due to their cost-effectiveness, versatility, and special physicochemical features (9).

Additive manufacturing processes, such as 3D printing, are based on computer-aided data sources and have resulted in tremendous convenience to technology today. Additive manufacturing attracts the attention of researchers and engineers in many fields, especially in medical applications, aerospace, spare part products, and others. The reasons are due to fast design, and final geometrical components can be produced in a short running time. Material extrusion-based additive manufacturing is especially suited for printing electrical components using various materials at a low cost. Additional machining processes are reduced or skipped entirely, while final costs and material waste are significantly reduced. The most prevalent approach in 3D printing is fused deposition modelling (FDM), which primarily uses a polymer filament (10). The filament will be heated at the extruder nozzle to ensure that the filament's plastic composite is in a semi-liquid condition. After that, the filament is extruded onto the platform or over previously printed layers. The thermoplastic nature of the polymer filament is critical for this process, as it allows the filaments to fuse during printing and then solidify at ambient temperature immediately (11). FDM builds a cross-sectional layer of extruded filament to form 3D geometry (12). Usually, materials used involve PLA, ABS, and polyetherimide.

This research aims to improve the properties of PLA reinforced with a conductive ZnO reinforcement filler produced by additive manufacturing. ZnO belongs to the class of transparent conducting oxides, which can be used as transparent electrodes in electronic devices (13). The RepRap Mendelmax 1.5 FDM 3D printer fabricated PLA and cPLA polymer composites. The impact of using precoated ZnO fillers was significant in this study. The performance of the composites was investigated using thermogravimetric analysis (TGA), FTIR, tensile testing, scanning electron microscopy (SEM) inspection, dynamic mechanical analysis, electrical impedance testing, and thermal conductivity testing.

2 Materials and methods

2.1 Raw materials

The raw materials used in this study were 1.75 mm-diameter PLA filaments (Cytron Technology Sdn Bhd), 1.75 mm-diameter cPLA filaments (Guangdong, China) and reagent-grade with ZnO powder ≥99% purity (Take It Global Sdn Bhd). ZnO was utilized without any further purification.

2.2 Composite fabrication

Before beginning the printing process, ZnO powder was mechanically ground for 30 min using a pestle and mortar to deagglomerate it. Twenty grams of PLA filaments (Cytron Technology Sdn Bhd) were thoroughly combined with 250 mL of acetone and stirred magnetically until PLA was completely dissolved. To keep the particles from settling to the bottom, ZnO powder was added to the PLA/acetone solution in 0.5:2 ratio with 5 mL of dispersion agents. Finally, the suspension was left at room temperature for 6 h.

The feedstocks for the FDM technique were PLA and carbon PLA filaments with a diameter of 1.75 mm. All specimens were printed at 0° raster angle and 100% infill density at a zigzag pattern by varying the content of ZnO fillers. The samples were printed in dog bone shapes for tensile testing in accordance with ASTM D638 by utilizing the open-source RepRap Mendelmax 1.5 FDM desktop 3D printer. The 3D printer was modified by attaching a filler dispenser near the extrusion nozzle. The movement or speed of the filler dispenser was regulated by altering the voltage provided to the controller, which was driven

by a DC motor. To achieve consistent filler distribution, the filler dispenser and extrusion nozzle worked concurrently during printing. The ZnO suspension was disseminated as a filler reinforcement into the PLA matrix in this investigation at three distinct dispenser speeds: 1,000, 1,400, and 1,800 rpm. Extruder temperatures of PLA and cPLA were set at 200°C and 230°C, respectively. The build plate temperature was fixed at 60°C for both samples with print cooling. FDM parameters like 0.2 mm layer height, 0° of top and bottom direction, 0.4 mm of nozzle diameter, and 70°C T_g of PLA were used during the experiment.

2.3 Characterization method

TGA was performed in a nitrogen environment using a thermogravimetric analyser (PerkinElmer, TGA7) at temperatures ranging from 25°C to 800°C with a heating rate of 10°C·min^{-1}. The proportion of the filler was introduced into the composites by changing the speed of the dispenser. TGA was used to evaluate the ZnO filler content of the composites in weight percentage (wt%). For cPLA containing carbon fibre, nitrogen gas was used to burn off PLA, and second, oxygen was used to burn off the carbon; thus, the final residue will be ZnO filler. A Perkin Elmer Spectrometer 2000 was used for FTIR measurements, and all the experiments were conducted at ambient temperature. The PLA, cPLA, PLA/ZnO, and cPLA/ZnO composites were selected for FTIR testing in this study to characterize the outcome. Tensile testing was performed on printed samples in accordance with ASTM D638 using a Universal Instron machine set at a crosshead speed of 5 mm·min^{-1} at room temperature. At least five samples for each ratio were tested. An SEM model JEOL JSM-6460LA instrument operating at 15 kV was used to evaluate the fracture surface morphology of pure and composite samples. To minimize the electrostatic charge built up during observation, the specimens were sputter-coated with platinum by utilizing a Quorum Q150R coater. A dynamic mechanical analyser (PYRIS Diamond DMA) was used to measure the storage and loss moduli of composites. The heating rate under continuous nitrogen flow was 5°C·min^{-1}. To perform the study, the procedures were conducted at 30–120°C. The samples were cut into rectangular shapes with dimensions of 50 mm × 45 mm × 1 mm under tension mode. An absolute axial heat flow approach was used to determine thermal conductivity. The data collected were utilized to calculate thermal conductivity using Eq. 1, where K is the thermal conductivity, x is the specimen thickness (1 mm), Q is the power, and A is the specimen area. The measured area, A, was 0.00024 m^2. The electrical impedance test was used to determine the electrical conductivity test. The samples were coated with conductive copper paste before the impedance test to guarantee electrical contact for the impedance measurement. An LCR meter (Hioki IM3522-50) measured the electrical characteristics at room temperature and a frequency range of 1,000 Hz to 100 kHz:

$$\kappa = \frac{Qx}{A\Delta T} \tag{1}$$

3 Results and discussion

TGA determined the ZnO suspension content (wt%) inside produced PLA composites. Figure 1 illustrates the thermograms of specimens printed at varied dispenser speeds, which were 1,000, 1,400, and 1,800 rpm.

The TGA curve revealed that PLA/ZnO and cPLA/ZnO decompose in a single stage and two stages, respectively. The deterioration of PLA began at about 270°C, as seen by the weight loss. The decomposition process was completed at almost 500°C with the remaining residue mass indicating the amount of ZnO filler incorporated into composites. Based on Figure 1, 11 wt% ZnO filler was dispensed onto the PLA with the high dispenser speed. During the printing procedure, 9 wt% and 7 wt% ZnO were dispensed on the composites at 1,400 and 1,000 rpm dispenser speeds, respectively. For cPLA, the thermal decomposition began at 290°C with a total mass loss of 60%. Switching the gas from nitrogen to oxygen at approximately 380°C resulted in carbon oxidation. When the dispenser speed was increased to medium or high, the filler amount was increased to 9.33 and 11 wt%, respectively. This demonstrated that the filler content could be regulated by adjusting the dispenser's motor speeds.

FTIR analysis is a technique to detect the presence of functional groups across the infrared spectrum of the PLA/ZnO composites. All the samples had almost identical FTIR spectra, implying that they have the same chemical composition and structure.

Figure 2 shows the structural comparison of pure PLA, cPLA, PLA/ZnO, and cPLA/ZnO composite spectra. The first peak found for both PLA samples and composites ranged between 3,577 and 3,700 cm^{-1}, and the second peak found fell in the range of 2,900–2,950 cm^{-1}. These first peaks indicate the presence of hydroxyl O–H stretching, while the second peaks are allocated to the stretching of C–H in both pure samples and composites. The 2,559.29 cm^{-1} region

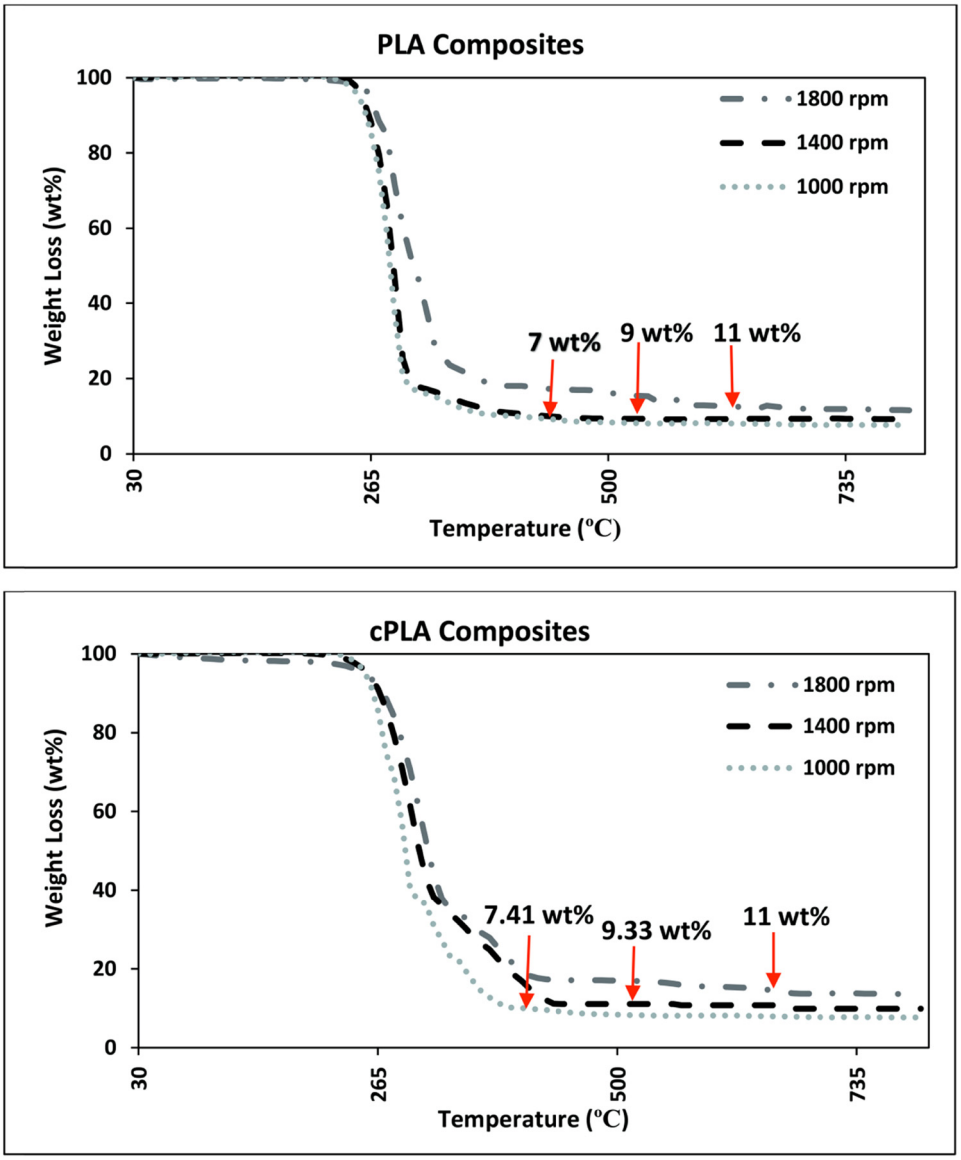

Figure 1: Thermograms for PLA and cPLA composites printing with different dispenser speeds.

band reflects the hydroxyl group by absorbing hydrogen on ZnO. There were peaks found at 2,012.44 and 2,171.11 cm^{-1} wavelengths for both samples, respectively, which were assigned to C≡C stretching, while the strong peaks for PLA located at 1,713 cm^{-1} range indicated the presence of C═O stretching vibration of the carbonyl group for the ester unit (14).

Next, the peaks at 1,451.59 and 1,364.60 cm^{-1} for pure PLA and PLA/ZnO composites were assigned to C–H deformation, which is symmetric and asymmetric bending, respectively. Additionally, the spectrum in the region of 1,080–1,260 cm^{-1} indicated the presence of strong C–O–C stretching (14). A huge shift occurred for PLA at 1,713 and 1,250 cm^{-1} due to the absence of ZnO reinforcement. The peak decrease for composites could be attributed to the interaction of ZnO in the pure PLA polymer matrix. Since ZnO accounts for a small part of the composites, its normal peaks are not as prominent as shown in Figure 2 (15). According to Figure 2, the absorption band at about 860 cm^{-1} corresponding to the C–C stretching showed evidence of amorphous phases of PLA contributing to the low density or disappearance of peaks (16). Overall, the FTIR spectra for the composites in the studied range practically revealed that the intensity of ZnO reinforcement did not change in any peaks in the PLA except for the peak at 3,450 cm^{-1} and assigned formation of secondary forces such as weak hydrogen bonds between the PLA polymer and ZnO (17). All PLA/ZnO composites exhibited a similar

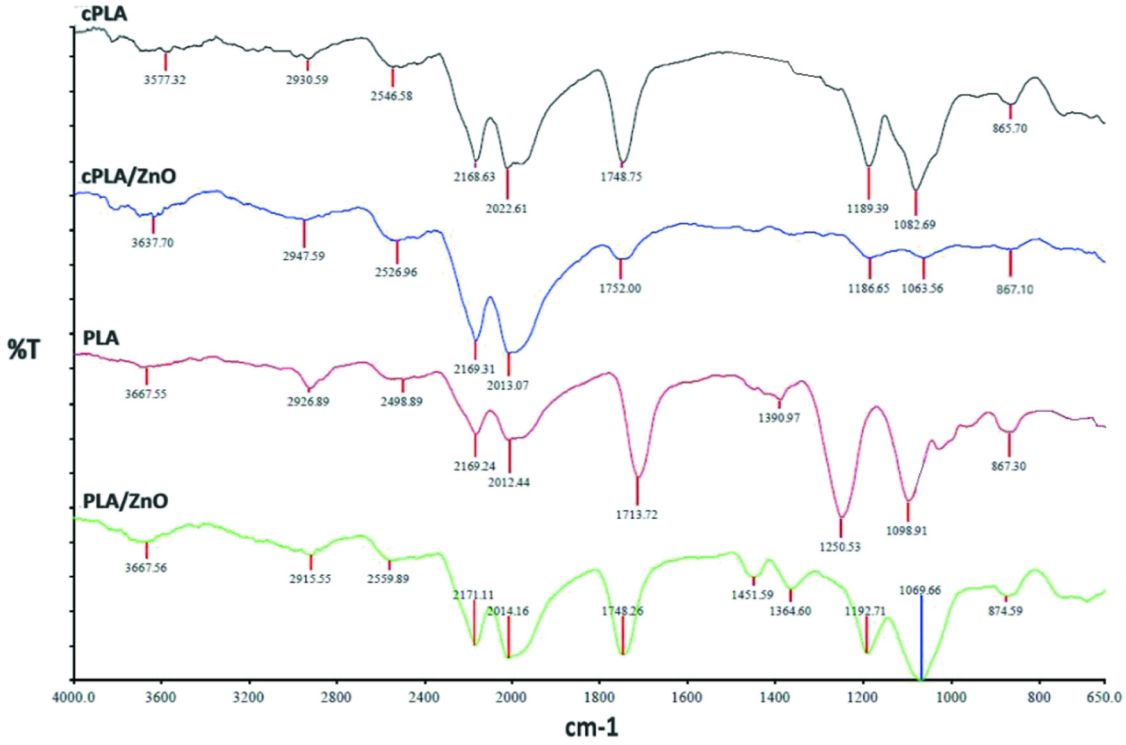

Figure 2: FTIR spectra of pure PLA, cPLA, PLA and cPLA composites.

band to pure PLA, with a less noticeable change in the peak area.

Figure 3 shows the effect of different ZnO loadings on the tensile strength of PLA and cPLA composites. The tensile strength increased progressively for PLA and slightly increased for cPLA as the filler loading increased, as seen in the graph. The tensile strength increased from 29.12 MPa to a maximum value of 39.50 MPa when filler loading increased to 11 wt%. The results revealed that the ZnO mixed well in PLA, implying that good interfacial adhesion

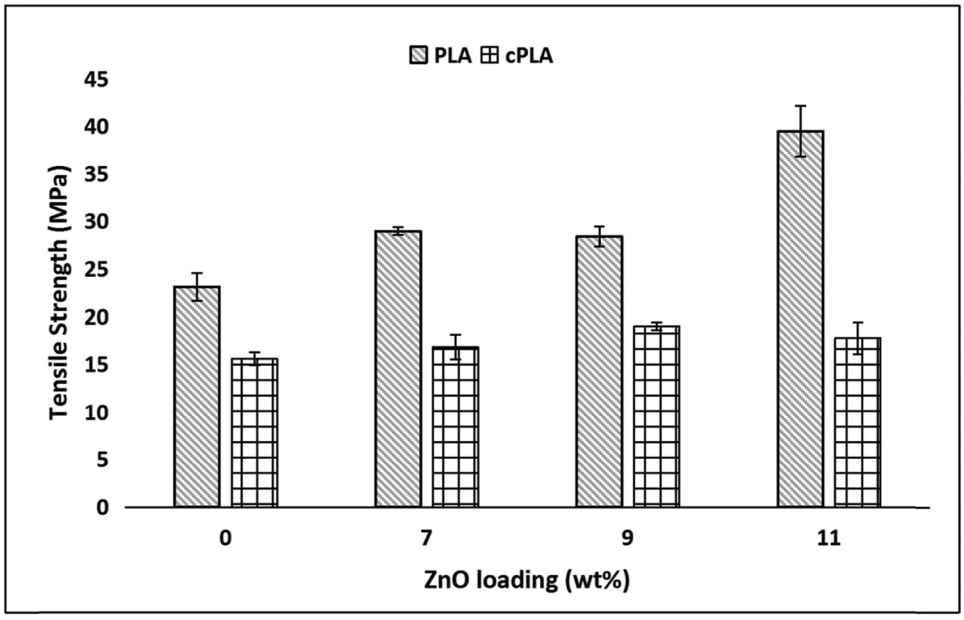

Figure 3: Effect of ZnO loading on tensile strengths of PLA/ZnO and cPLA/ZnO composites.

will facilitate effective stress transfer. This is owing to the tensile load being transferred to the filler before it fails (18).

However, pure PLA and the cPLA control sample have low tensile strength compared to all the composites. This illustrates ductility behaviour because the pure samples had minimal stress to fracture the samples. The tensile strength of the cPLA composite is significantly lower than that of PLA. This is because of the weak bonding between carbon, PLA, and ZnO. Initially, the carbon fibre dispersed well into the PLA filament. The cPLA filament melted at the same melting temperature as the original PLA during printing. It will develop the cluster formation of carbon when PLA is in the molten state and results in carbon fibre that is no longer uniformly dispersed (18). Adding ZnO will hinder cluster attachment and finally cause secondary agglomeration (19). There was a slight increase in tensile strength when the ZnO loading increased

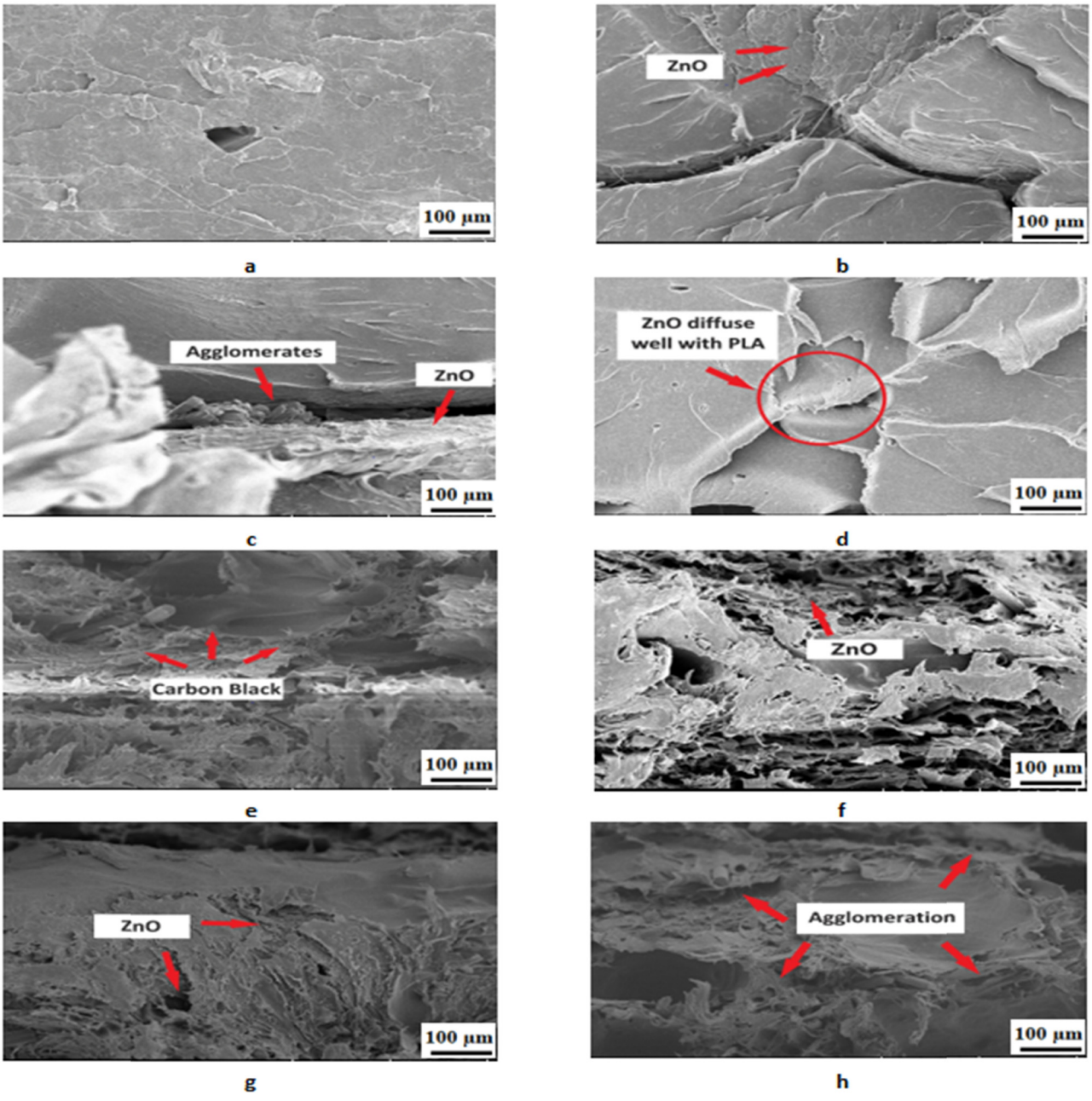

Figure 4: (a) SEM micrographs of the pure PLA sample, (b) PLA sample with 4 wt% ZnO, (c) PLA sample with 7 wt% ZnO, (d) PLA sample with 11 wt% ZnO, (e) pure cPLA sample, (f) cPLA sample with 4 wt% ZnO, (g) cPLA sample with 7 wt% ZnO, and (h) cPLA sample with 11 wt% ZnO.

to 9 wt% and dropped when it reached 11 wt%. This is because when ZnO filler reaches a high population, non-homogeneous ZnO induces the lump and agglomeration making stress transmission from matrix to fibre complicated and disrupting the matrix phase's continuity (20). This was proven by the SEM micrograph, as shown in Figure 4.

Figure 4b and c shows the SEM micrograph of PLA printed with 7 and 9 wt% ZnO fillers. ZnO fillers diffused effectively inside the PLA matrix and produced adhesion with the PLA interface, as demonstrated in Figure 4d. There was an increase in the tensile strength for all composites filled with ZnO fillers compared to the unfilled control samples (Figure 4a). When the filler loading was

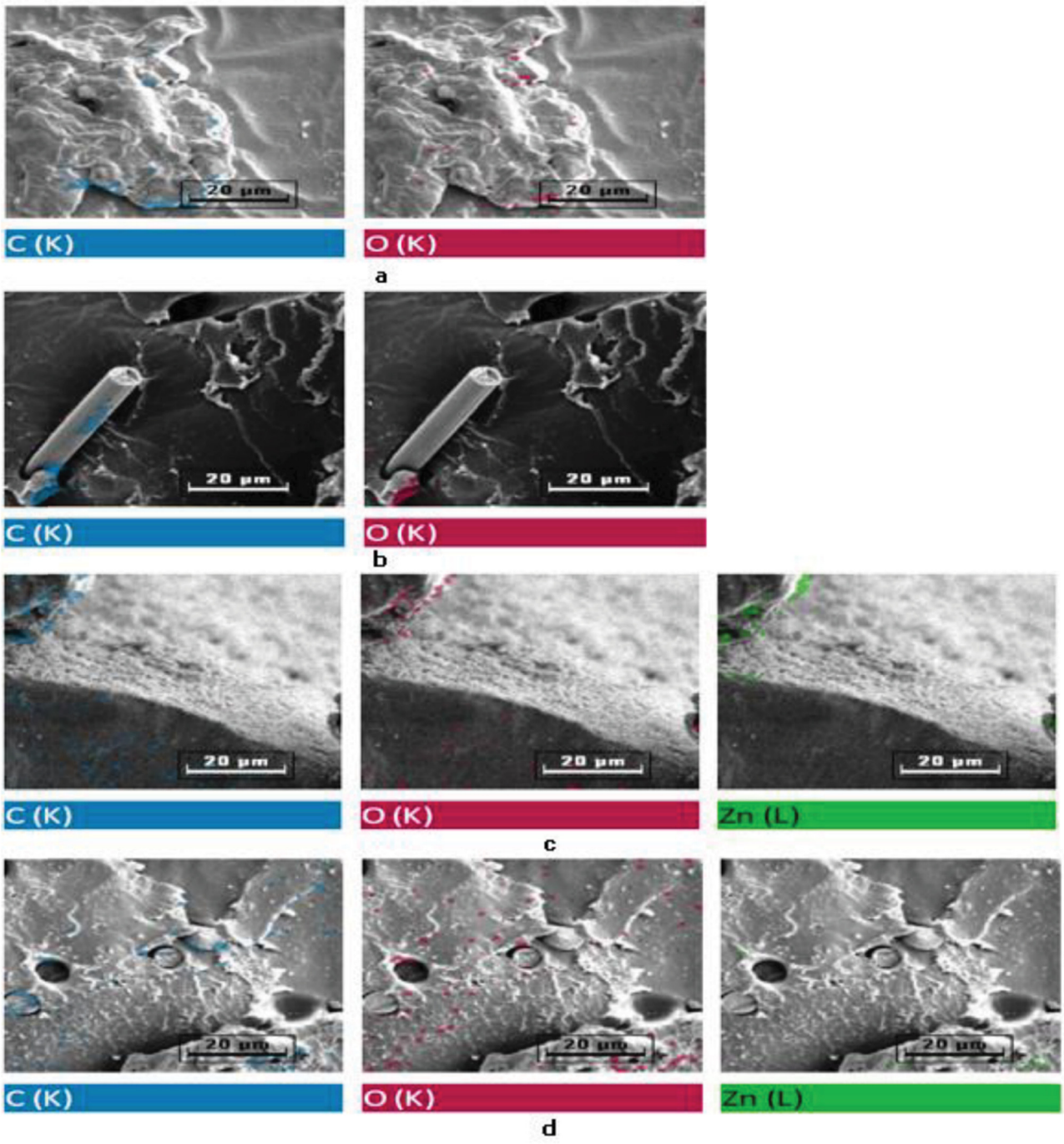

Figure 5: (a) Elemental mapping of pure PLA sample, (b) pure cPLA sample, (c) PLA sample with 11 wt% ZnO, (d) cPLA sample with 4 wt% ZnO.

increased to 9 wt%, the tensile strength decreased by 1.5%. This is because when filler loading was increased to a critical level, non-homogeneous ZnO fillers are expected to induce agglomerates, which generate a stress concentration zone that causes cracking and finally weakens the tensile strength of PLA composites (21). The PLA reinforced with 11 wt% ZnO filler achieved the maximum tensile strength due to the strengthening impact of the filler on the composites, as shown in Figure 4d (22).

Based on previous studies, Alig et al. investigated the effect of filler arrangement and agglomeration on the mechanical, electrical, and thermal characteristics of a CNT-filled composite (23). Due to poor dispersion in the polymer matrix, first or primary agglomerates developed during the CNT manufacturing process. Secondary agglomerates (agglomerates formed as a result of secondary processing, such as melt mixing, extrusion, or injection moulding) formed inside the composites due to non-Brownian diffusion of particles having attractive interactions. The tensile characteristics degraded by the presence of secondary agglomerates that were more loosely packed (23). Initial agglomerates formed during the printing process when PLA was heated to its melting temperature, resulting in poor carbon black (CB) dispersion inside PLA. When the ZnO filler solution was applied, there will be a lack of bonding because the temperature decrease leads to a loss in tensile strength. The SEM micrograph showed the formation of agglomerates in Figure 4h, while Figure 4e illustrates well dispersion of CB in PLA samples.

Elemental mapping is required to understand the distribution of fillers and the concurrence with the explanation given previously. The presence of ZnO filler distribution was confirmed in composites, as shown in Figure 5c and d.

Figure 6 shows the effect of ZnO loading on the tensile modulus of the PLA and cPLA composites. Filled PLA had a greater tensile modulus than unfilled PLA. When the filler content increased, the tensile modulus increased from 1,247.18 to 1,578.08 MPa. At 11 wt% ZnO loading, the maximum value of 1.58 GPa was achieved. The tensile modulus of cPLA composites demonstrated a similar trend to PLA due to the stiffening role of fillers. Fillers functioned as obstacles that restricted the polymer chains from moving freely and therefore reduced the flexibility of the composites (18). Filler rigidity increased the modulus and contributed to the ability to tolerate deformation. Furthermore, the cPLA composites had lower tensile modulus than the PLA composites with the same filler amount. This may be due to the carbon fibre creating the uneven arrangement of clusters resulting in the loss of adhesion between the reinforcer and matrix, thus reflecting the reduced stiffness (24).

Kumar et al. studied the effects of alumina filler concentration on Young's modulus of the ABS/alumina composite (25). The alumina loading varied from 1 to 5 vol% within ABS. At a filler loading of 5 vol%, the modulus increased by 9% compared to that of pure ABS. The concentration of particles filled between the polymer chain

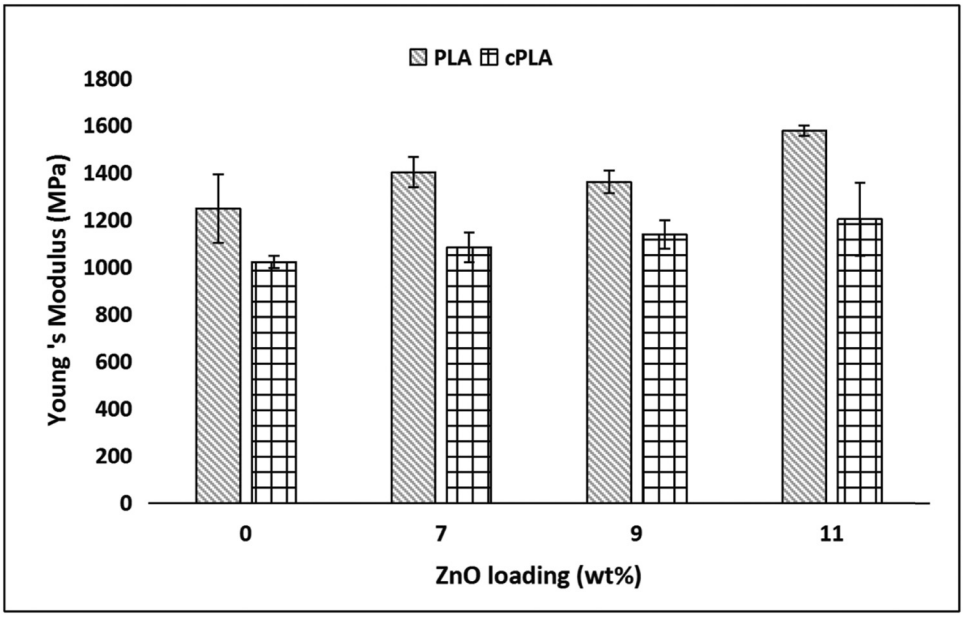

Figure 6: Effect of ZnO loading on Young's modulus of PLA/ZnO and cPLA/ZnO composites.

was much higher and thus the polymer chain segment would deform itself in a less mobile manner, accounting for the higher Young's modulus. The results were similar to the experimental results, which showed that with 11 wt% loading, the moduli of PLA/ZnO and cPLA/ZnO increased by 27% and 18%, respectively (26).

Figure 7 demonstrates the effect of different ZnO loadings on the dynamic storage moduli, E', of PLA and cPLA composites. The storage modulus reduced dramatically when temperature increased, and there was a significant drop in the T_g region. At the same temperatures, the storage moduli of PLA and cPLA composites were greater than those of pure PLA and cPLA. At all temperatures, the storage moduli increased as the filler loading increased, and the composite with the highest filler loading, PLA and cPLA reinforced with 11 wt% ZnO, had the highest E' value. This was linked to the inclusion of stiffness improvement with the filler addition (27). The fillers reinforcing impact and strong matrix/filler interaction boosted the composites' overall rigidity (20).

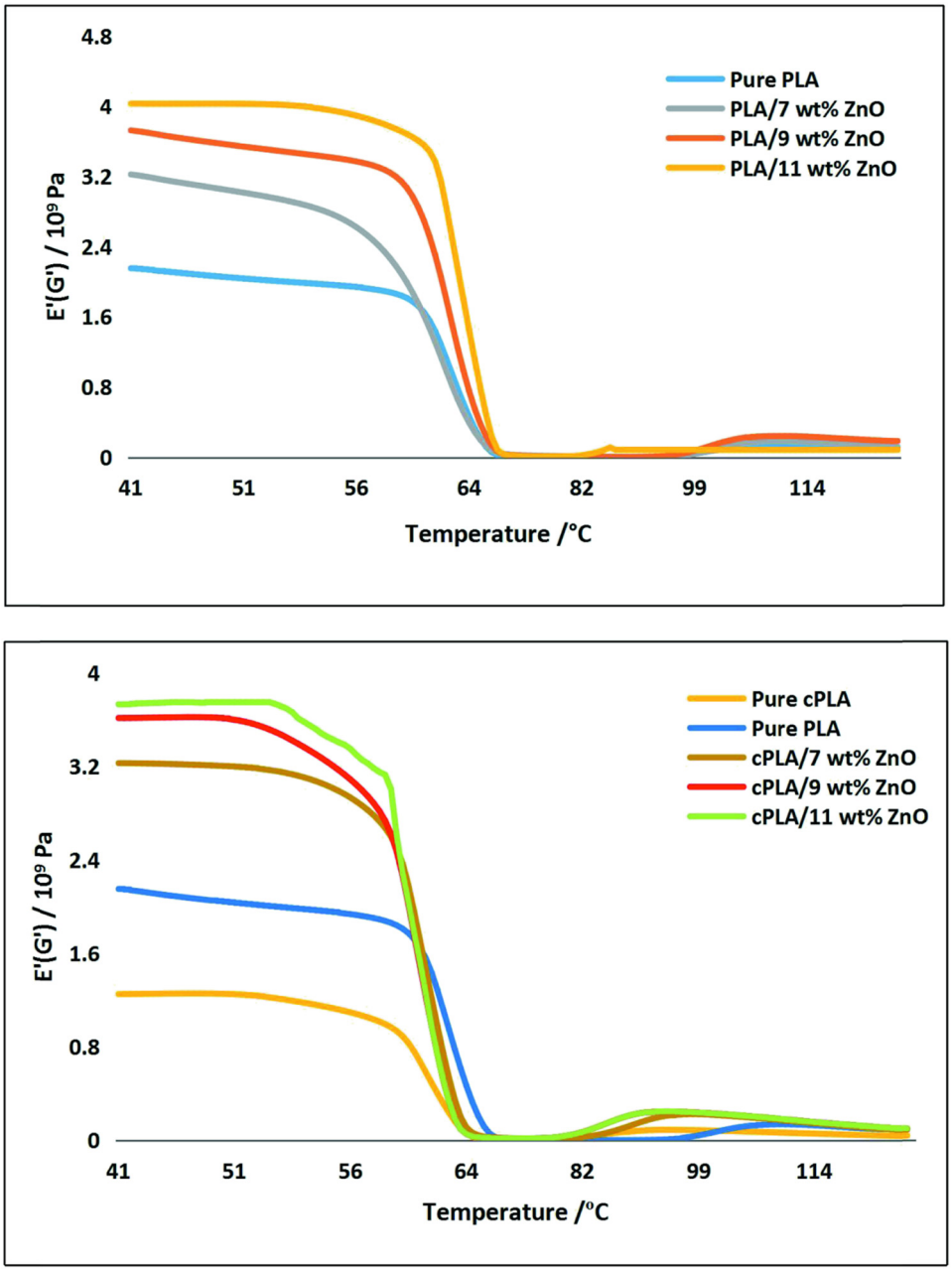

Figure 7: Dynamic storage moduli (E') of PLA/ZnO and cPLA/ZnO.

This inhibited the mobility of molecular chains of the matrix, thus increasing the stiffness of the composite materials (28).

However, cPLA/ZnO composites had a lower E' than PLA/ZnO composites due to the presence of CB and ZnO clusters, which lowered the material's stiffness. According to previous studies, Santos et al. discovered a similar result when they investigated the characteristics of ABS reinforced with titanium dioxide (TiO_2) and CB. The agglomerate formation was found to be a fault that caused stiffness deterioration. Because of the inadequate interaction between CB and TiO_2 in the ABS matrix, a better degree of stress transfer at the boundary became impossible (29).

Figure 8 displays the effect of different ZnO loadings on the dynamic loss moduli, E'', of PLA and cPLA composites. The curve representing the loss modulus remains constant at low temperatures and increases gradually until reaching the peak value because intermolecular bonding is destroyed (30). It was observed that the loss modulus decreased continuously after the highest peak as the mobility of the chain improved. Owing to the decrease in stiffness, more energy is dissipated; therefore, the highest loss modulus is observed for less rigid samples (31). The reduction in the intensity of the matrix chains' motion is associated with an increase in T_g. At the same temperature, the loss modulus of composites with

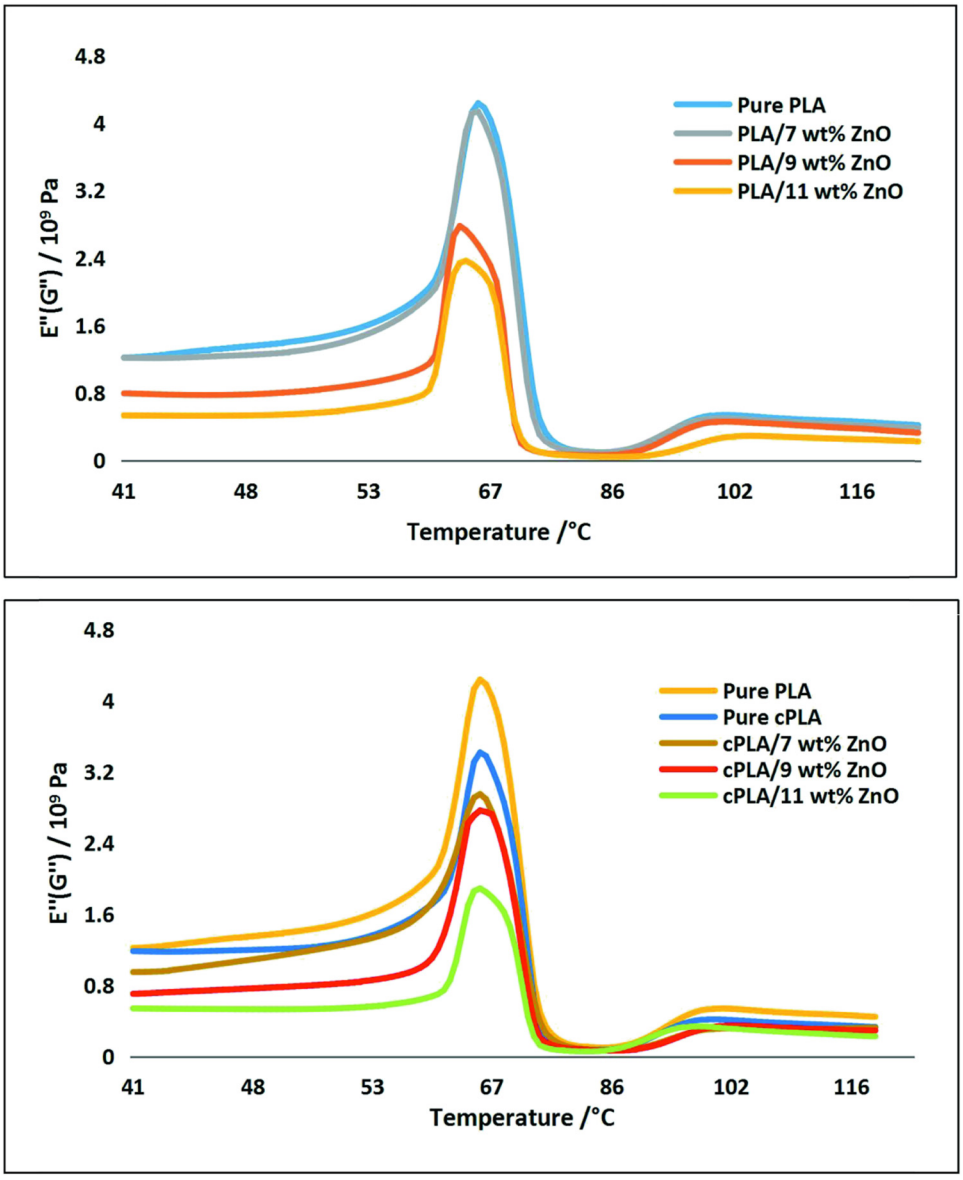

Figure 8: Loss moduli (E'') of PLA/ZnO and cPLA/ZnO composites.

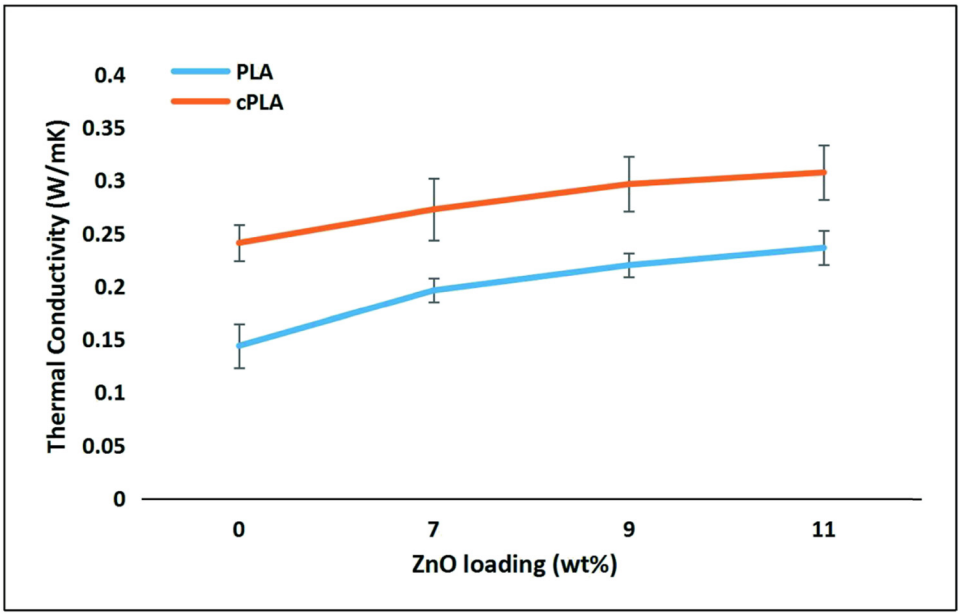

Figure 9: Thermal conductivity of PLA and cPLA composites.

increasing filler loading was lower. This might be owing to the polymer chain's constrained mobility, which results in less energy being dissipated due to the chain restriction. The result showed that the loss modulus tends to lose energy, which is inversely proportional to the storage modulus (31).

Figure 9 shows the increasing trend in thermal conductivity when the ZnO loading increased from 7 to 11 wt% for both composites. This is owing to the use of a filler with a higher thermal conductivity than the PLA matrix, which causes higher heat dissipation between the ZnO filler and the PLA matrix. The maximum thermal conductivity was attained by 11 wt% cPLA, which was 0.3074 $W{\cdot}mK^{-1}$, while the lowest reading was acquired by pure PLA, which was 0.1412 $W{\cdot}mK^{-1}$. Because the matrix acts as a thermal barrier for heat propagation, more fillers will mix well with PLA and produce conductive pathways to transport heat rapidly (32). As we can see, when the ZnO filler is increased, the thermal conductivity of PLA composites increases from 0.1962 to 0.2361 $W{\cdot}mK^{-1}$, indicating that more filler particles are packed together to generate effective close contact between them and form conductive pathways (33). Due to naturally high thermal conductivity CB, the thermal conductivity of cPLA composites was greater than that of PLA composites (34). Fillers are well dispersed inside the polymer matrix at 7 and 9 wt%. Some fillers developed agglomerates at larger 11 wt% filler loadings, promoting quick heat conduction and increasing thermal conductivity at 0.3074 $W{\cdot}mK^{-1}$ (32). This can be proved through SEM micrographs Figure 4h reveals the generation of agglomerates inside the composites. This is similar to the result of previous studies, which found that CB particles formed conductive clusters and networks in the poly(ethylene-oxide) polymer matrix when the sample approached the percolation threshold, therefore improving thermal conductivity (35).

Figure 10 shows a comparison of the impedance testing of PLA/ZnO and cPLA/ZnO composites. The 7 wt% of cPLA composite had the highest impedance at 10 kHz frequency. This is due to the CB component in cPLA. The electrical conductivity of PLA/ZnO and cPLA/ZnO composites steadily enhanced with the inclusion of ZnO fillers. When the fillers achieved their percolation threshold value, conductive networks of ZnO formed within the matrix (36). CB and ZnO filler generated a high electrically conductive network, facilitating carrier mobility inside the polymer chains and hence decreasing the impedance of materials (37). The previous research stated that PLA has low permittivity due to its small polarization of the macromolecules (38). Among the polymer, epoxy was used due to its high impedance properties. However, epoxy has low toughness. Previous research stated that the impedance in zinc-rich epoxy was 80 $\Omega{\cdot}cm^2$ at 100,000 Hz (39). All PLA/ZnO and cPLA/ZnO composites had lower impedance when frequency increased. Therefore, cPLA/ZnO was suitable for replacing epoxy composites. According to Abdalhadi et al., the matrix of OPEFB/PLA with Fe_2O_3 filler was homogeneous and the number of voids was reduced (38). Therefore, suitable ZnO suspension content was also an important factor that could influence the properties of composites.

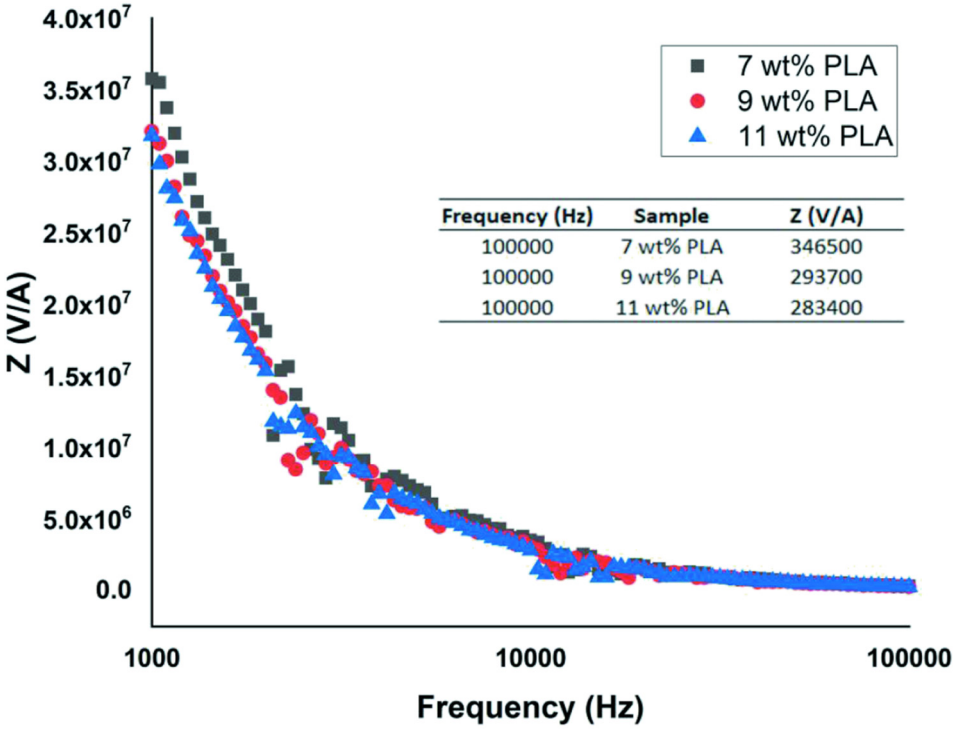

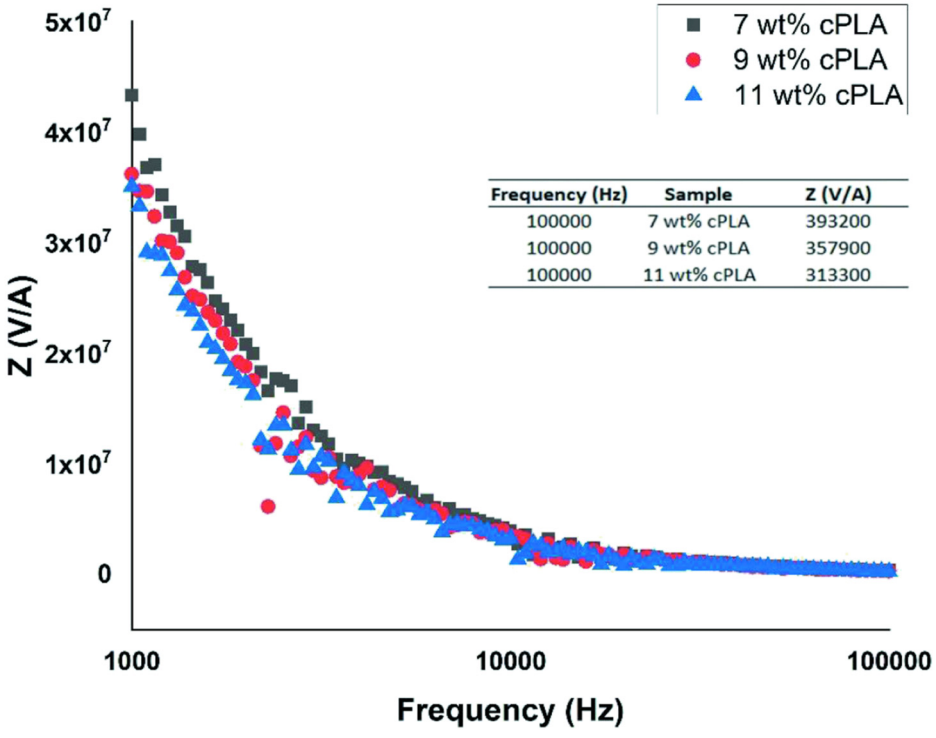

Figure 10: Impedance testing of PLA/ZnO and cPLA/ZnO composites.

4 Conclusions

This study shows that the 11 wt% PLA/ZnO composites have the highest mechanical properties which are tensile strength and Young's modulus. According to the results, the mechanical properties of the samples with filler addition were greater than those of the pure samples. These enhancements were made possible by improving the interfacial adhesion between the PLA matrix and the ZnO suspension. Because of the stiffening effect and high strength of the ZnO suspension, tensile strength and Young's modulus were improved by incorporating ZnO into the PLA matrix. The detailed morphology can be achieved by SEM analysis due to the uniform diffusion of ZnO in the PLA, indicating excellent interfacial adhesion that will facilitate effective stress transfer. This eventually leads to high tensile strength and dynamic mechanical properties. Because of the existence of CB and ZnO clusters, cPLA/ZnO composites have a lower E' but higher E'' than PLA/ZnO composites. In addition, the inherent high thermal and impedance of cPLA/ZnO compared to those of pure and PLA composites is due to the incorporation of the carbon fibre and conductive ZnO into PLA. This is because the formation of a conductive path between them transmits heat and electricity quickly. Our approach expands the good mechanical, electrical, and thermal conductivity performances by integrating the ZnO suspension into PLA to provide superior-quality electrical instruments for the future.

Acknowledgement: The authors thank the Faculty of Chemical Engineering Technology, University Malaysia Perlis (UniMAP) for providing the research and testing facilities.

Funding information: The authors would like to acknowledge the support from the Fundamental Research Grant Scheme (FRGS) under a grant number of FRGS/1/2018/TK05/UNIMAP/02/14 from the Ministry of Higher Education Malaysia.

Author contributions: Mei Ai Tan: writing – original draft, writing – review and editing, methodology, formal analysis; Cheow Keat Yeoh: writing – review and editing; Pei Ling Teh: project administration; Nor Azura Abdul Rahim: resources; Cheah Chie Song: visualization.

Conflict of interest: The authors state no conflict of interest.

References

(1) Hagen R. A comprehensive reference||polylactic acid. Polym Sci. 2012;231–6. doi: 10.1016/b978-0-444-53349-4.00269-7.
(2) Vasile C, Rapa M, Stefan M, Stan M, Macavei S, Darie-Nita RN, et al. New PLA/ZnO:Cu/Ag bionanocomposites for food packaging. Express Polym Lett. 2017;11(7):531–44. doi: 10.3144/expresspolymlett.2017.51.
(3) Liang L, Huang T, Yu SX, Cao WW, Xu TT. Study on 3D printed graphene/carbon fiber multi-scale reinforced PLA composites. Mater Lett. 2021;300(6):130173. doi: 10.1016/J.MATLET.2021.130173.
(4) Ning F, Cong W, Hu Y, Wang H. Additive manufacturing of carbon fiber-reinforced plastic composites using fused deposition modeling: Effects of process parameters on tensile properties. J Compos Mater. 2017;51(4):451–62. doi: 10.1177/0021998316646169.
(5) Al Zahmi S, Alhammadi S, El Hassan A, Ahmed W. Carbon fiber/PLA recycled composite. Polymers. 2022;14:2194. doi: 10.3390/polym14112194.
(6) Ning F, Cong WL, Hu ZL, Huang K. Additive manufacturing of thermoplastic matrix composites using fused deposition modeling: A comparison of two reinforcements. J Compos Mater. 2017;51(27):3733–42. doi: 10.1177/0021998317692659.
(7) Weng Z, Wang J, Senthil T, Wu L. Mechanical and thermal properties of ABS/montmorillonite nanocomposites for fused deposition modeling 3D printing. Mater Des. 2016;102:276–83. doi: 10.1016/j.matdes.2016.04.045.
(8) Sudeepan J, Kumar K, Barman TK, Sahoo P. Study of mechanical and tribological properties of ABS/clay polymer composite using Taguchi optimization method. J Manuf Technol Res. 2014;6(3/4):153–75.
(9) Diani J, Liu Y, Gall K. Finite strain 3D thermoviscoelastic constitutive model. Polym Eng Sci. 2006;46(4):486–92. doi: 10.1002/pen.20497.
(10) Ngo TD, Kashani A, Imbalzano G, Nguyen KTQ, Hui D. Additive manufacturing (3D printing): A review of materials, methods, applications and challenges. Compos Part B Eng. 2018;143:172–96. doi: 10.1016/j.compositesb.2018.02.012.
(11) Mohamed OA, Masood SH, Bhowmik JL. Optimization of fused deposition modeling process parameters: A review of current research and future prospects. Adv Manuf. 2015;3(1):42–53. doi: 10.1007/s40436-014-0097-7.
(12) Dehghanghadikolaei A. Additive manufacturing as a new technique of fabrication. J Sci Eng Res. 2018;5(8):123–31. doi: 10.14302/issn.2831-8846.j3dpa-18-2207.
(13) Lim JH, Yeoh CK, Abdullah C, Teh PL. Band structure and thermoelectric properties of inkjet printed ZnO and ZnFe2O4 thin films. Ceram Int. 2016;42(10):12064–73. doi: 10.1016/j.ceramint.2016.04.135.
(14) Chu Z, Zhao T, Li L, Fan F, Qin Y. Characterization of antimicrobial poly (lactic acid)/nano-composite films with silver and zinc oxide nanoparticles. Materials (Basel). 2017;10(6):659. doi: 10.3390/ma10060659.
(15) Brounstein Z, Yeager CM, Labouriau A. Development of antimicrobial PLA composites for fused filament fabrication. Polymers. 2021;13(4):580. doi: 10.3390/polym13040580.

(16) Szyma M, Chyli M, Pieczywek PM, Walkiewicz A, Pertile G, Frac M, et al. Evaluation of nanocomposite made of polylactic acid and nanocellulose from carrot pomace modified with silver nanoparticles. Polymer. 2020;12(4):812. doi: 10.3390/polym12040812.
(17) Junpha J, Wisitsoraat A, Prathumwan R, Chaengsawang W, Khomungkhun K, Subannajui K. Electronic tongue and cyclic voltammetric sensors based on carbon nanotube/polylactic composites fabricated by fused deposition modelling 3D printing. Mater Sci Eng C. 2020;117:111319. doi: 10.1016/j.msec.2020.111319.
(18) Hamzah KA, Yeoh CK, Noor MM, Teh PL, Aw YY, Sazali SA, et al. Mechanical properties and thermal and electrical conductivity of 3D printed ABS-copper ferrite composites via 3D printing technique. J Thermoplast Compos Mater. 2019;35:1–14. doi: 10.1177/0892705719869405.
(19) Aw YY, Yeoh CK, Idris MA, Teh PL, Elyne WN, Hamzah KA, et al. Influence of filler precoating and printing parameter on mechanical properties of 3D printed acrylonitrile butadiene styrene/zinc oxide composite. Polym Plast Technol Eng. 2018;58(1):1–13. doi: 10.1080/03602559.2018.1455861.
(20) Yang Z, Peng H, Wang W, Liu T. Crystallization behavior of poly(ε-caprolactone)/layered double hydroxide nanocomposites. J Appl Polym Sci. 2010;116(5):2658–67. doi: 10.1002/app.31787.
(21) Fu Y, Feng XQ, Lauke B, Mai YW. Effects of particle size, particle/matrix interface adhesion and particle loading on mechanical properties of particulate-polymer composites. Compos Part B Eng. 2008;39(6):933–61. doi: 10.1016/j.compositesb.2008.01.002.
(22) Tian XY, Liu TF, Wang QR, Dilmurat Q, Li DC, Ziegmann G. Recycling and remanufacturing of 3D printed continuous carbon fiber reinforced PLA composites. J Clean Prod. 2017;142(4):1609–18. doi: 10.1016/j.jclepro.2016.11.139.
(23) Alig I, Potschke P, Lellinger D, Skipa T, Pegel S, Kasaliwal GR, et al. Establishment, morphology and properties of carbon nanotube networks in polymer melts. Polymer. 2012;53(1):4–28. doi: 10.1016/j.polymer.2011.10.063.
(24) Chigondo F, Shoko P, Nyamunda BC, Moyo M. Maize stalk as reinforcement in natural rubber composites. Int J Sci Technol Res. 2013;2(6):263–71.
(25) Kumar V, RamKumar J, Aravindan S, Malhotra SK, Vijai K, Shukla M. Fabrication and characterization of ABS nano composite reinforced by nano sized alumina particulates. Int J Plast Technol. 2009;13(2):133–49. doi: 10.1007/s12588-009-0011-5.
(26) Mehraein H. Impact of process parameters on mechanical properties of 3D printed polycaprolactone parts. Master Science: Wichita State University; 2018.
(27) Margem FM, Monteiro SN, Neto JB, Rodriguez RJS, Soares BG. The dynamic-mechanical behavior of epoxy matrix composites reinforced with ramie fibers. Rev Mater. 2010;15(2):167–71. doi: 10.1590/S1517-70762010000200012.
(28) Manoharan S, Suresha B, Ramadoss G, Bharath B. Effect of short fiber reinforcement on mechanical properties of hybrid phenolic composites. J Mater. 2014;2014:1–9. doi: 10.1155/2014/478549.
(29) Santos RM, Botelho GL, Machado AV. Development of acrylonitrile-butadiene-styrene composites with enhanced UV stability. J Mater Sci. 2014;49(2):510–8. doi: 10.1007/s10853-013-7728-4.
(30) Abu-Abdeen M. Static and dynamic mechanical properties of poly(vinyl chloride) loaded with aluminum oxide nanopowder. Mater Des. 2012;33(1):523–8. doi: 10.1016/j.matdes.2011.04.059.
(31) Arivazhagan A, Masood SH. Dynamic mechanical properties of ABS material processed by fused deposition modelling. Int J Eng Res Appl. 2012;2(3):2009–14.
(32) Kochetov R, Korobko AV, Andritsch T, Morshuis PHF, Picken SJ, Smit JJ. Modelling of the thermal conductivity in polymer nanocomposites and the impact of the interface between filler and matrix. J Phys D Appl Phys. 2011;44(39):395401. doi: 10.1088/0022-3727/44/39/395401.
(33) Nikzad M, Masood SH, Sbarski I. Thermo-mechanical properties of a highly filled polymeric composites for fused deposition modeling. Mater Des. 2011;32(6):3448–56. doi: 10.1016/j.matdes.2011.01.056.
(34) Tsekmes IA, Kochetov R, Morshuis PHF, Smit JJ. Thermal conductivity of polymeric composites: A review. Proceeding IEEE International Conference on Solid Dielectric (ICSD); 2013 June 30-July 4. Bologna, Italy. Netherlands; 2013. p. 678–81.
(35) Elimat ZM, Al-Hussami SA, Zihlif AM. Effect of carbon black on the thermoelectrical properties of poly(ethylene-oxide) composites. J Compos Mater. 2013;47(28):3525–34. doi: 10.1177/00219983124672.
(36) Park W, Hu J, Jauregui LA, Ruan X, Chen YP. Electrical and thermal conductivities of reduced graphene oxide/polystyrene composites. Appl Phys Lett. 2014;104(11):113101. doi: 10.1063/1.4869026.
(37) Ju H, Kim M, Kim J. Enhanced thermoelectric performance of highly conductive poly(3,4-ethylenedioxythiophene)/carbon black nanocomposites for energy harvesting. Microelectron Eng. 2015;136:8–14. doi: 10.1016/j.mee.2015.03.030.
(38) Abdalhadi DM, Abbas Z, Ahmad AF, Matori KA, Esa F. Controlling the properties of OPEFB/PLA polymer composite by using Fe_2O_3 for microwave applications. Fibers Polym. 2018;19(7):1513–21. doi: 10.1007/s12221-018-8118-y.
(39) Du XM, Xu PJ, Cong PL, Zhou ZJ. Compatibilization and toughness modification of linear aliphatic epoxy compound on paving epoxy asphalt. Mater Struct. 2020;53(2):1–12. doi: 10.1617/s11527-020-01473-0.